1   Post-Insemination Selection Dominates Pre-Insemination Selection in Driving Rapid Evolution
2   of Male Competitive Ability
3
4
5   Short Title: Post-Insemination Selection Drives Male Evolution
6
7

8   Katja R. Kasimatis[1,#a]*, Megan J. Moerdyk-Schauwecker[1], Ruben Lancaster[1], Alexander Smith[1],
9   John H. Willis[1], and Patrick C. Phillips[1]*
10
11   [1]Institute of Ecology and Evolution, University of Oregon, Eugene, Oregon, United States of
12   American
13
14   [#a]Current address: Department of Ecology and Evolutionary Biology, University of Toronto,
15   Toronto, Ontario, Canada
16
17   *Corresponding authors:
18   Email: k.kasimatis@utoronto.ca (KRK)
19   Email: pphil@uoregon.edu (PCP)
20

Abstract

Sexual reproduction is a complex process that contributes to differences between the sexes and divergence between species. From a male's perspective, sexual selection can optimize reproductive success by acting on the variance in mating success (pre-insemination selection) as well as the variance in fertilization success (post-insemination selection). The balance between pre- and post-insemination selection has not yet been investigated using a strong hypothesis-testing framework that directly quantifies the effects of post-insemination selection on the evolution of reproductive success. Here we use experimental evolution of a uniquely engineered genetic system that allows sperm production to be turned off and on in obligate male-female populations of *Caenorhabditis elegans*. We show that enhanced post-insemination competition increases the efficacy of selection and surpasses pre-insemination sexual selection in driving a polygenic response in male reproductive success. We find that after 30 generations post-insemination selection increased male reproductive success by an average of 5- to 7-fold. Contrary to expectation, enhanced pre-insemination competition hindered selection and slowed the rate of evolution. Furthermore, we found that post-insemination selection resulted in a strong polygenic response at the whole-genome level. Our results demonstrate that post-insemination sexual selection plays a critical role in the rapid optimization of male reproductive fitness. Therefore, explicit consideration should be given to post-insemination dynamics when considering the population effects of sexual selection.

Introduction

Sexual selection drives the evolution of some of the most remarkable phenotypes observed in nature. Interest in these flashy phenotypes has led to a focus on studying pre-insemination reproductive dynamics, such as male-male competition and female choice [1]. However, in animals with internal fertilization, reproduction is more complex and requires a series of interactions within and between the sexes to produce a viable offspring. From a male's perspective, total reproductive success can be partitioned into successfully winning a mating event and then successfully winning a fertilization event. Therefore, sexual selection has the potential to act on both the variance in mating success and the variance in fertilization success (also referred to as gametic selection [2,3]). We do not know if selection during these

2

51 reproductive phases interacts in an additive, antagonistic, or synergistic manner to optimize total

52 male reproductive success. Understanding this balance is critical not only for quantifying male

53 reproductive fitness within a generation, but also for understanding how sexual selection shapes

54 the evolution of reproductive success over time. Such processes are critical for relating the role

55 of sexual selection to population adaptation [4,5] and divergence [6].

56   Experimental separation of sexual selection before and after mating within an adaptive

57 framework has proved extremely challenging. Previous studies have taken the approach of

58 Arnold and Wade [7] to partition the variance in total reproductive success into the variance in

59 mating success and the variance in fertilization success [reviewed in 8]. These studies have

60 inferred mixed results as to opportunity for sexual selection. Several studies suggest that the

61 variance in mating success comprises greater than 95% of the total variance in reproductive

62 success [9,10], while others indicate a greater contribution of the post-insemination phase [11-

63 15]. Additionally, evolutionary analyses of seminal fluid proteins show a high opportunity for

64 post-insemination selection [16,17]. While informative, the opportunity for sexual selection does

65 not necessarily translate into realized selection, which contributes to the lack of consistent

66 patterns between studies. Moreover, this framework is an indirect approach for partitioning

67 reproductive success and thus lacks the ability to connect the action of selection to the

68 underlying genomic response to understand how reproductive success is evolving.

69   *Caenorhabditis elegans* is an ideal system for disentangling mating interactions. First, the

70 mating system in *C. elegans* can be manipulated to prevent hermaphrodite self-sperm production

71 and create functional females that rely on male-female mating. Males in these populations have

72 low reproductive success relative to males from obligate outcrossing *Caenorhabditis* species

73 [18], which creates a high opportunity for the evolution of reproductive success. Second, we

74 have developed an external, non-toxic sterility system for *C. elegans* [19] that capitalizes on the

75 auxin-inducible degron system to degrade the critical spermatogenesis gene *spe-44* and

76 effectively turn off sperm production. The induction of sterility allows for sperm competitive

77 dynamics to be isolated from male-male competitive dynamics for thousands of worms at a time.

78 Finally, *C. elegans* is amenable to the evolve and re-sequence experimental approach [20,21],

79 which allows us to not only quantify the impact of sexual selection on reproductive success, but

80 also identify the underlying genetic structure of the traits involved.

3

81   Here we capitalize on transgenics to isolate the contributions of pre-insemination mating

82   competition versus post-insemination sperm competition to the evolution of reproductive fitness

83   of a newly derived *C. elegans* male population. We first create an obligate outcrossing *C.*

84   *elegans* population composed of functional females and males with inducible sterility. We then

85   performed 30 generations of replicated experimental evolution using a factorial design that

86   partitions sexual selection due to within-strain and between-strain competitive dynamics

87   occurring during pre-insemination and post-insemination. This experiment explicitly tests if pre-

88   insemination sexual selection and post-insemination sexual selection contribute to reproductive

89   success in an additive, synergistic, or antagonistic manner. If pre- and post-insemination

90   selection are additive or synergistic, then we expect to see the greatest increase in total

91   reproductive success when competition is enhanced through the addition of external male

92   competitors during both reproductive stages. Alternatively, if these phases are antagonistic such

93   that competition is beneficial during one stage but detrimental during the other, then we expect to

94   see a reduction in total reproductive success when competition is enhanced during both

95   reproductive stages. We can infer the source of antagonistic competition by comparing-and-

96   contrasting the effects of enhanced and reduced post-insemination competition.

97

Results

Factorial framework to isolate selection on mating and fertilization success

101   We designed an experimental evolution framework that controls pre- and post-insemination

102   competitive interactions using three distinct and powerful genetic manipulations: a mutation in

103   the sex determination pathway (*fog-2*) to disrupt self-sperm production in hermaphrodites and

104   maintain obligate male-female mating [18], targeted degradation of a key spermatogenesis

105   protein (*spe-44*) to control male mating duration [19], and an inducible lethal marker (*peel-1*) to

106   eliminate offspring from competitor males [22]. To generate a selective event, male sterility was

107   induced after an initial mating period (Fig 1). Increased sperm competition was then generated

108   by adding competitor males from a different strain. After a 24 hour competitive phase, progeny

109   were collected, hatched, and then heat-shocked to induce lethality of the competitor male cross-

110   progeny, leaving only those progeny from the evolving males to start the next generation. This

4

111 design isolates sperm competitive success from male mating success and selects for sperm

112 defensive capability and longevity.

113   The induction of sterility and addition of competitor males generated a factorial

114 experimental design resulting in four experimental evolution regimes (Fig 2A). When both

115 sterility was introduced and competitors subsequently added (between-strain post-insemination

116 only competition, BS-PO), there was increased sexual selection on post-insemination fertilization

117 dynamics. Alternatively, when only sterility was induced, and competitor males not added

118 (within-strain post-insemination only competition, WS-PO), evolving males experienced reduced

119 sperm competition and potentially decreased post-insemination sexual selection. To represent the

120 full degree of sexual selection acting on pre- and post-insemination competition (between-strain

121 pre- and post-insemination competition, BS-P&P), sterility was not induced, but competitor

122 males were added. Finally, no direct sexual selection was applied when neither sterility was

123 induced nor competitors added (within-strain pre- and post-insemination competition, WS-P&P).

124 The WS-P&P regime represents the base level of sexual selection experienced by recently

125 derived *C. elegans* males.

Opportunity for selection is high in the ancestral population

127 We used multiple rounds of low-dose EMS mutagenesis to generate genetic variation in the

128 ancestral population (Fig S1). Based on the mutation rate of EMS per generation [23], at least

129 937,500 non-exclusive mutations were expected to be segregating in the post-mutagenesis

130 population prior to lab adaptation. We observed 321,929 SNPs segregating in the ancestral

131 population, suggesting strong purifying selection during the pre-experimental evolution lab

132 adaptation period (Fig S1). The ancestral population had a genome-wide mean nucleotide

133 diversity of $\pi = 0.06$ and the minor allele frequency ranged from 0.004 to 0.5 (Fig S2A-D; File

134 S1). These diversity estimates are higher than those commonly observed in *C. elegans* and are

135 more comparable to the obligate outcrossing species *C. remanei* [24]. The distribution of variants

136 was relatively even across chromosome domains, unlike the characteristic pattern of higher

137 diversity on the chromosome arms when compared to the chromosome center [25-27] (Fig S2C-

138 D; File S2). SNP density, however, reflected this chromosome arm-center pattern: the mean SNP

139 density on chromosome arms was $\theta_w = 0.004$ and in chromosome centers was $\theta_w = 0.002$ (Fig

140 S2E-F). Despite the X chromosome having a slightly higher recombination rate in the small

141 chromosome center domain [25] coupled with a greater opportunity for purifying selection in

142   males, the X did not have the lowest SNP density (mean $\theta_w = 0.0027$) as expected. Instead,

143   chromosome I had a significantly lower mean SNP density (mean $\theta_w = 0.0012$; $t = -67$, $p <$

144   0.001) than the other chromosomes. Together these summary statistics indicate that the ancestral

145   population had more segregating genetic variants than is commonly observed in *C. elegans*,

146   though much of this diversity is not in the gene dense chromosome centers.

147   We quantified ancestral reproductive success under highly competitive conditions

148   occurring during both pre- and post-insemination (i.e., total reproductive success) and during

149   post-insemination alone using a novel male competitor (Fig 2B). Total reproductive success was

150   slightly, though significantly, poorer than the null expectation of equal competitive ability

151   between ancestral male and competitor male backgrounds (proportions test: $\chi^2 = 6.87$, d.f. = 1, p

152   < 0.01, 95% C.I. of ancestral competitive success = 40.4–48.6%). Ancestral male sperm

153   competitive ability was especially poor with an average of 4.1% of progeny coming from

154   ancestral males relative to the competitor (proportions test: $\chi^2 = 863$, d.f. = 1, p < 0.0001, 95%

155   C.I. of ancestral sperm competitive success = 3.0–5.5%). Therefore, in the ancestral population

156   post-insemination success only contributed 9.2% to the overall reproductive success of males

157   (Fig 2C). The poor reproductive success of ancestral males under competitive conditions

158   indicates the opportunity for selection – particularly gametic selection – to improve male

159   competitive ability was high.

Post-insemination selection drove evolutionary change in males

161   We quantified total reproductive success for each replicate population after 10 selective events

162   occurring over 30 generations of evolution under the same highly competitive conditions used to

163   assay the ancestral males. The contribution of post-insemination increased across all evolved

164   replicates relative to the ancestor, such that on average post-insemination success contributed

165   26.7% to 34.7% of total male reproductive success (Fig 2C). The BS-P&P and WS-PO regimes

166   trended towards a higher fraction of total reproductive success that could be attributed to post-

167   insemination success across replicate means, suggesting that enhanced post-insemination

168   competition positively affects fertilization success. Interestingly, post-insemination contribution

169   increased to 79.7% in a single BS-P&P replicate. This evolutionary increase was due to a 13-fold

170   increase in post-insemination success and only a 1.4-fold increase in total reproductive success.

171   Overall, the increased contribution of post-insemination dynamics was driven by the

172   significant increase in post-insemination reproductive success of evolved males compared to

6

173 ancestral males (Fig 2D; WS-P&P: z-value = 3.7, p < 0.001; BS-P&P: z-value = 3.6, p = 0.001;

174 WS-PO: z-value = 3.4, p = 0.002; BS-PO: z-value = 4.0, p < 0.001). Once again, the BS-PO

175 regime showed the strongest evolutionary response with a 6.8-fold increase from the ancestor,

176 which supports the hypothesis that enhanced post-insemination competition increases the

177 efficacy of sexual selection. Additionally, the WS-PO regime – the regime with the lowest levels

178 of post-insemination competition – comparatively showed the lowest mean evolutionary change

179 from the ancestor, though overall the evolutionary response was still strong. However, a post hoc

180 test to determine if experimental evolution under directed sexual selection increased the rate at

181 which post-insemination evolved relative to the WS-P&P baseline conditions showed no

182 significant difference between regimes, suggesting a strong underlying selective pressure on

183 sperm competitive ability.

184   Total reproductive success of evolved males compared to ancestral males also increased

185 significantly across regimes (WS-P&P: z-value = 4.7, p < 0.001; BS-P&P: z-value = 2.7, p =

186 0.02; WS-PO: z-value = 3.5, p < 0.001; BS-PO: z-value = 3.6, p < 0.001), though to a lesser

187 extent than post-insemination success alone (Fig 2D). Interestingly, only the BS-P&P regime

188 showed a significant effect of sexual selection (z = -3.6, p < 0.001) compared to the baseline

189 WS-P&P regime. Contrary to expectation [5,28], enhanced pre-insemination competition

190 reduced the evolutionary response in male reproductive success. The WS-PO and BS-PO were

191 not significantly different from the baseline. Thus, increasing the opportunity for pre-

192 insemination sexual selection did not lead to faster evolution. Rather, enhanced pre-insemination

193 competition appeared to hinder the rate of evolution of male reproductive success.

Effective population size reflects strong selection

195 The effect population size (N_e) ranged from 16% to 24% of the census size (N = 5,000) across all

196 replicates and regimes (Fig S3; File S3). Regimes where post-insemination interactions were

197 isolated had on average lower effective population sizes across all chromosomes than the WS-

198 P&P and BS-P&P regimes. However, there was no significant effect of regime on N_e (ANOVA:

199 F = 0.72, d.f. = 3, p = 0.54). Variance in reproductive success impacts N_e, especially when the

200 sex ratio of breeding individuals is skewed. We calculated the upper bound on the number of

201 breeding males [29], under the assumption that all females reproduced and the reduction in

202 population size was due to variance in male reproductive success alone. For the estimated N_e

203 range, this analysis suggests that only 222-333 males reproduced (8.9-13.3% of the census male

204 population), supporting strong sexual selection acted on males.

205   Given the XX/XO chromosomal sex determination system of *C. elegans*, we expected the

206 estimated effective population size of the X chromosome to be approximately 75% of the

207 estimated effective population size of the autosomes. The effective population size was

208 significantly different between the autosomes and sex chromosome (t = 3.34, d.f. = 24.5, p <

209 0.01). However, contrary to expectation, the mean effective population size estimated using X

210 chromosome SNPs was 1.9 times larger than that estimated using autosomal SNPs.

Sperm competitive ability is a polygenic trait

212 We fit two complementary models to determine if the frequency of alleles at each SNP changed

213 from the ancestral population to the evolved population in each regime. Model 1 used a post hoc

214 approach to compare SNP counts in the evolved and ancestral populations (Model 1: glm(SNP ~

215 regime), linear hypothesis test: Anc – Evolved$_{regime}$ = 0) and identified 3,461 significant SNPs

216 after a Bonferroni correction (p < 7.43e-6). The significance trends of Model 1 (File S4) support

217 the more robust findings of Model 2 (File S5). Here we fit independent models for each regime

218 that included sampling at two intermediate generations (Model 2: glm(SNP$_{regime}$ ~ time)). In

219 Model 2, we identified 160 non-overlapping significance peaks across the five autosomes and the

220 X chromosome, indicating that male reproductive success is polygenic (Fig 3, File S6).

221 Significance peaks showed a strong chromosome arm-center structure, likely driven by the

222 higher density of SNPs on the chromosome arms (Fig S2). Thirty-one peaks were shared across

223 all regimes (Fig 3, Fig S4). The BS-PO regime had the highest number of significant SNPs (n =

224 1,994) as well as the highest number of unique significance peaks (n = 32). The WS-PO regime

225 and the shared WS-PO and BS-PO regimes represent the third and fourth highest groupings,

226 reinforcing that isolated gametic sexual selection resulted in a strong polygenic genomic

227 response (Fig S4). The WS-P&P regime had the fewest number of significance peaks and only

228 three peaks were unique to this regime.

229   Linkage disequilibrium was low between SNPs and significance peaks could be narrowed

230 down to small genomic regions (File S6). The median peak width was 362.5 base pairs. The

231 largest peak spanned a 10,753 base pair region on the right arm of Chromosome I and lies in the

232 intron of gene C17H1.2 (Fig S5). This gene exhibits male-biased expression, though its function

233 is uncharacterized [30]. The majority of significance peaks (n = 108) fell within a genic region,

234 while 26 peaks were intergenic (File S6). Twenty-three peaks were located in pseudogenes and

235 an additional three peaks overlapped with coding genes and pseudogenes.

236   To determine the functional pathways underlying improved male reproductive success,

237 we examined the gene ontology (GO) terms associated with the genes underlying significance

238 peaks (Fig S6; File S6). The most common molecular function identified was SCF ubiquitin

239 ligase complex formation through F-box proteins (n = 16). Several genes were also related to

240 each carbohydrate binding, G-coupled protein receptor activity, and transferase transporter

241 activity. Six genes were associated with some form of RNA. However, 47.5% of genes were

242 uncharacterized in function, identifying a lack of male-specific functional knowledge.

243

244 # Discussion

245 Quantifying the balance of pre- and post-insemination selection is critical for understanding how

246 male reproductive fitness is comprised and how reproductive success evolves. This knowledge

247 translates to better understanding how sexual selection contributes to population adaptation. We

248 took a direct approach to isolate post-insemination from pre-insemination dynamics by coupling

249 transgenic induction systems within an experimental evolution framework to examine whether

250 these reproductive phases contribute in an additive or antagonistic manner to male reproductive

251 fitness. All treatments showed a strong, rapid response to selection at both the phenotypic and

252 genomic levels (Fig 2 and 3). Phenotypic results indicate that post-insemination selection was the

253 major driver of male evolution. Genomic results support the importance of post-insemination

254 selection and suggest that selection during this phase increased the efficacy of selection.

255 Additionally, reproductive success is a highly polygenic trait with genes on all chromosomes

256 contributing to the response to selection. These results provide new insights on the complexity of

257 post-insemination dynamics and highlight the importance of considering all phases of

258 reproduction.

259   The balance between pre- and post-insemination selection was complex and depended on

260 the strength of selection imposed. At the phenotypic level, the within-strain competition

261 treatments suggest that pre- and post-insemination act in an additive manner to increase male

262 reproductive fitness (Fig 2). However, this pattern does not hold under enhanced between-strain

263 competitive conditions. Instead, contrary to expectation, increased male-male competition (BS-

264 P&P) decreased the rate of adaptation relative to base levels (WS-P&P). These increased

265   competitive interactions could potentially harm females as a byproduct (i.e., sexual conflict) and
266   therefore reduce female reproductive rate. However, the BS-PO treatment had the same number
267   of males attempting to mate with females as the BS-P&P, the difference being that the BS-PO
268   males could not transfer sperm post-mating. Thus, the increased number of males actually
269   inseminating females is likely the contributing source of the decreased evolutionary response.
270   While it seems possible that increased competition among sperm led to the decrease in fecundity
271   [31], it is also possible that females altered egg-laying rates in response to the amount of sperm
272   present as a result of a resource trade-off between reproductive and maintenance functions. To
273   our knowledge, no studies have quantified this relationship in nematodes.
274   In contrast, increased sperm competition appeared to improve the rate of adaptation in
275   males. BS-PO males trended towards the highest rate of increase in post-insemination success
276   and post-insemination contributed the most to their overall reproductive response. While these
277   comparative trends were not significant at the phenotypic level, at the genomic level populations
278   evolved under increased sperm competition had the strongest genomic response across dozens of
279   genes (Fig 3 and S4). Interestingly, populations evolved under reduced sperm competitive
280   dynamics (WS-PO) also showed a strong genomic response, suggesting that isolating post-
281   insemination dynamics from pre-insemination dynamics allowed sexual selection to act more
282   efficiently. While we isolated post-insemination through transgenic induction, this type of effect
283   could be seen in nature if females were to mate with males over distinct periods of time and store
284   sperm for later use.
285   Our method of population construction generated little haplotype structure, which
286   allowed us to map genetic elements that responded to selection with high precision. A challenge
287   in many quantitative trait loci [32] and evolve-and-resequence studies [33] is narrowing down
288   the regions of selection to make specific statements on the genetic architecture of traits. In
289   contrast, here we have high confidence that reproductive success and sperm competitive success
290   are complex traits underlaid by over 60 genes (Fig 3 and S4). In most cases, we were able to
291   narrow the region under selection to just a few hundred base pairs. While this precision should in
292   principle allow us to identify the causal basis of the genetic response, given the highly polygenic
293   structure of these complex traits, each contributing gene likely contributes a small effect, which
294   makes the next step of functional molecular characterization challenging. To help prioritize this
295   process, we performed a GO analysis to look for patterns in molecular functions or biological

296 processes (Fig S6). F-box proteins involved in protein-protein interactions, such as ubiquitin-
297 ligase complex formation [34], showed a strong response in all treatments. Though their exact
298 function is unknown, many of the several hundred *C. elegans* F-box genes show signatures of
299 positive selection in wild isolates, suggesting that selective conditions observed in nature were
300 mimicked in the lab [35]. However, nearly half of the identified genes were uncharacterized in
301 function, despite *C. elegans* being a major model system. These genes represent a candidate list
302 for future molecular studies to characterize the networks underlying male reproductive function.
303 In particular, gene C17H1.2 is of interest for future study as it has a large significance peak
304 falling within the second intron and exhibits male-biased expression patterns.

305 Sexual selection has a large effect on population size by limiting the number of
306 successfully breeding adults [reviewed in 36]. We estimated the effective population size to be
307 less than one quarter of the enforced census size. If one assumes that nearly all females are mated
308 as an upper bound, this difference suggests that on average approximately 10% of males sired all
309 offspring (Fig S3). This is the very definition of opportunity for sexual selection [7] and is
310 consistent with our conclusion that strong sexual selection acted on these populations even in the
311 base level treatment (WS-P&P). Interestingly, the effective population size of the X chromosome
312 was larger than expected given the XX/XO sex determination system of *Caenorhabditis*
313 nematodes, which would suggest that the effective population size of the X chromosome should
314 be 3/4 that of the autosomes under neutral expectations. The flip in the N_e ratio between the X
315 and autosomes is further evidence that the response to selection is driven by sexual interactions
316 among males, as the X chromosome is in males 1/3 of the time while autosomes are in males 1/2
317 the time, and so the autosomes are more susceptible to drift induced by variance in mating
318 success specially among males [36,37]. Interestingly, the X chromosome also had the fewest
319 number of significance peaks, so in addition to the demography of the X chromosome itself, it is
320 also possible that there may be additional reductions in autosomal variation due hitchhiking [36].

321 Darwin first noted that the existence of elaborate sex-specific traits seemed at odds with
322 regular evolutionary processes, and more than a hundred of years of research has subsequently
323 focused on understanding how sexual selection drives diversity for these traits within and
324 between populations. Our work indicates that the cryptic phenotypes and molecular effects that
325 emerge during post-insemination interactions are equally important in determining fertilization
326 success and likely to be just as genetically complex.

11

327

Materials and methods

Molecular biology

330 Guides targeting sequences in the same intergenic regions utilized by the ttTi4348 and ttTi5605

331 MosSCI sites have been previously described [19,38]. Additional guide sequences were chosen

332 using the Benchling CRISPR design tool, based on the models of Doench *et al*. [39] and Hsu *et*

333 *al*. [40], and the Sequence Scan for CRISPR tool [41]. Guides were inserted into pDD162

334 (Addgene #47549) [42] using the Q5 site-directed mutagenesis kit (NEB) or ordered as

335 cr:tracrRNAs from Synthego. A complete list of guide sequences can be found in Table S1.

336 Repair template plasmids were assembled using the NEBuilder HiFI Kit (NEB) from a

337 combination of restriction digest fragments and PCR products. PCR products were generated

338 using the 2x Q5 PCR Master Mix (NEB) in accordance with manufacturer instructions. Details

339 of plasmid construction can be found in the supplemental methods and Tables S2 and S3.

340 Plasmids were purified using the ZR Plasmid Miniprep kit (Zymo) and all plasmid assembly

341 junctions were confirmed by Sanger sequencing.

Strain generation

343 All strains used in this study are listed in Table S4 and depicted schematically in Figure S1.

344 Insertion of transgenes was done by CRISPR/Cas9 using standard methods. Briefly, a mixture of

345 10ng/μl repair template plasmid, 50ng/μl plasmid encoding CAS9 and the guide RNA and

346 2.5ng/μl pCFJ421 (Addgene #34876) [43] was injected into the gonad of young adult

347 hermaphrodites. Where hygromycin resistance (HygR) was used as a selectable event, two to

348 three days after injection, hygromycin B (A.G. Scientific, Inc.) was added to the plates at a final

349 concentration of 250μg/ml. Successful insertion was confirmed by PCR and Sanger sequencing.

350 To generate the male sterility induction strain PX624, *pie-1p*::*TIR-1* was inserted into the

351 Chromosome I site and a degron tag was added to the native *spe-44* locus of JU2526 as in

352 Kasimatis *et al.* [19] (Fig S1A, C). The majority of exons 2-4 of the native *fog-2* gene were then

353 deleted using the guides and oligonucleotide repair template listed in Table S1 and Table S3.

354 Microinjections and *dpy-10* co-marker screening were done as previously described [19,44]. This

355 strain represents the predecessor for the experimental evolution ancestral population (see

356 "Generating genetic diversity").

357   The *hsp-16.41p::PEEL-1 + rpl-28p::mKate2 + rps-0p::HygR* three gene cassette was

358   inserted into the Chromosome I site of CB4856. Individuals with confirmed inserts were crossed

359   to JK574, containing *fog-2*(q71), and backcrossed 4 times to CB4856 (Fig S1B). A single pair

360   was then chosen for 14 generations of inbreeding to create strain PX626. To introduce a second

361   copy of *hsp-16.41p*::*PEEL-1*, a *hsp-16.41p*::*PEEL-1 +loxP::rps-0p::HygR::loxP* two gene

362   cassette was inserted into the Chromosome II site (Fig S1). The HygR gene was then removed by

363   injection of a CRE expressing plasmid pZCS23 [45] at 10ng/μl, with removal monitored by

364   PCR, to generate PX630. PX626 was crossed to PX630 to generate the final novel, bioassay

365   competitor strain PX631 (Fig S1E).

366   To generate a lethality and male sterility induction strain, PX624 was crossed with

367   PX631 and then backcrossed 5 times with PX624 to introgress *hsp-16.41p*::*PEEL-1* in the

368   Chromosome II site to create strain PX655. Since the Chromosome I site of PX624 is occupied

369   by *pie-1p*::*TIR-1*, CRISPR/Cas9 was used to insert the *hsp-16.41p::PEEL-1 + rpl-28p::mKate2*

370   *+ rps-0p::HygR* three gene cassette into PX624 at a site on Chromosome III between *nac-3* and

371   K08E5.5 that has not been previously used for transgene insertion, creating PX656. PX655 and

372   PX656 were then crossed to create the final competitor strain PX658 (Fig S1D).

Generating genetic diversity

374   The male sterility induction strain (PX624) was exposed to ethyl methanesulfonate (EMS) to

375   induce genetic variation (Fig S1). Populations of 8,000-10,000 age-synchronized L4 worms were

376   divided into 4 technical replicates and suspended in M9 buffer. Worms were incubated in 12.5

377   mM EMS for 4 hours at 20ºC, after which they were rinsed in M9 buffer and plated on NGM-

378   agar plates. Replicate populations were given two recovery and growth generations with ample

379   food following a mutagenesis event. A total of five low-dose mutagenesis rounds coupled with

380   recovery generations were performed. During each of the recovery rounds, a subset of worms

381   from each replicate were screened on NGM-agar plates containing 1 mM indole-3-acetic acid

382   (Auxin, Alfa Aesar) following Kasimatis *et al*. [19] to test if mutagenesis had compromised the

383   integrity of the sterility induction system. Specifically, if eggs were observed on an auxin-

384   containing plate, then that replicate was removed and another replicate was subdivided, so a total

385   of four replicate populations were always maintained.

386   After the final round of mutagenesis and recovery, replicate populations were maintained

387   for five generations of lab adaptation. They were then combined for an additional 10 generations

13

388   of lab adaptation with a population size of approximately 30,000 worms. The integrity of the

389   sterility induction system continued to be screened every two generations throughout the entire

390   lab adaptation process. This genetically diverse, male sterility induction strain PX632 represents

391   the ancestral experimental evolution population (Fig S1).

Experimental design and worm culture

393   The ancestral population (PX632) was divided into four experimental regimes, which varied

394   based on total (i.e., pre- and post-insemination) or sperm (i.e., post-insemination) competition

395   dynamics occurring either within the evolving strain alone or between the evolving strain and

396   competitor strain (PX658): within-strain pre- and post-insemination competition (WS-P&P),

397   within-strain post-insemination only competition (WS-PO), between-strain pre- and post-

398   insemination competition (BS-P&P), and between-strain post-insemination only competition

399   (BS-PO).

400   Each regime had six replicate populations and experimentally evolved for 30 generations.

401   Ten selective events occurred over the course of experimental evolution denoted by the induction

402   of sterility, the addition of competitors, and the induction of sterility and addition of competitors

403   in the WS-PO, BS-P&P, and BS-PO regimes, respectively (Fig 1 & Fig 2A). The WS-P&P had

404   no direct selection applied. Each selective event was followed by a recovery generation, where

405   no direct selection was applied, to allow the populations to return to the census size. During the

406   recovery generation, a subset of worms from the regimes with sterility induction were screened

407   on auxin-containing plates to ensure the sterility induction system was functional. Additionally, a

408   subset of worms from all replicates was frozen for future stocks. The detailed selection

409   procedure follows.

410   To start each selective event age synchronized L1 worms were plated onto five 10 cm

411   NGM-agar plates seeded with OP50 *Escherichia coli* at 20ºC with a density of 1,000 worms per

412   plate, giving a census size of 5,000 worms per replicate per regime [46,47]. Forty-eight hours

413   later, experimental regimes with sterility induction (WS-PO and BS-PO) were transferred to

414   NGM-agar plates containing 1mM auxin. Experimental regimes without sterility induction (WS-

415   P&P and BS-P&P) were transferred to fresh NGM-agar plates. For all transfers, worms within a

416   replicate were pooled and then redistributed across five plates with a density of 1,000 worms per

417   plate. After 24 hours, males from the competitor strain PX658 were filter-separated from females

418   using a 35 um Nitex nylon filter and added to experimental regimes with competition at a mean

14

419   density of 200 competitor males per plate (evolving to competitor ratio of 1:2.5). After another

420   24 hours, eggs were collected from all replicates, hatched, and age synchronized. To ensure that

421   only progeny from the evolving males and not from the competitor males were being propagated,

422   larval lethality of competitor progeny was induced following Seidel *et al.* [22]. Briefly,

423   approximately 5,000 L3 worms were suspended in 5 mL of S-Basal and heat-shocked in a 35ºC

424   sealed water bath for 2.5 hours to activate ectopic expression of the lethal protein PEEL-1. After

425   heat-shock, worms were plated on NGM-agar plates to end the selective event. All experimental

426   regimes were subjected to the heat-shock procedure, even if competitor worms were not added.

427   A subset of approximately 200 worms from the competition and sterility and competition

428   regimes were removed prior to heat-shock and fluorescence screened to determine the proportion

429   of progeny coming from the competitor worms, which expressed red fluorescent protein (RFP),

430   versus the evolving worms, which had no fluorescence.

431   The competitor strain PX658 was maintained on NGM-agar plates seeded with OP50 *E.*

432   *coli* at 20ºC in population sizes of approximately 20,000 worms. The competitor strain was reset

433   from freezer stocks every 3 weeks (~4 generations) to prevent adaptation and maintain a constant

434   competitive phenotype.

Fertility assays

436   We assayed the fertility of the ancestor and all the evolved replicates (N = 13 populations) to

437   determine the total competitive reproductive success of males as well as their sperm competitive

438   success. The assay conditions mimicked the environment under which worms evolved. Total

439   competitive reproductive success was assessed by adding the novel competitor PX631 in equal

440   proportion to evolving males. Sperm competitive success was assessed by inducing sterility of

441   the evolving male before adding the novel competitor in equal proportion to evolving males. The

442   use of the novel competitor and high competition ratio acted as a "stress-test" of male

443   competitive ability. Both assays were performed with a population of 250 evolving females, 250

444   evolving males, and 250 novel competitors. After a 24-hour competition period, eggs were

445   collected, hatched, and age synchronized for screening. At least 200 L3 progeny were counted

446   for each assay and then fluorescence-screened for the proportion of progeny coming from

447   evolving (RFP minus) or competitor (RFP plus) males. Three independent biological replicates

448   were done for each assay across all experimental evolution replicates (File S7).

15

449   Fertility data were analyzed using the R statistical language v4.0.0 [48]. An equality of

450   proportions test was performed on the ancestral data to determine if ancestral males sired half the

451   total progeny under total competitive and sperm competitive conditions. The evolved male

452   fertility data were analyzed using a linear model (GLM) framework with random effects using

453   the *lme4* v.1.13 package [49]. The *multcomp* package [50] was then used to perform a planned

454   comparisons tests with defined contrasts to determine if: i) evolutionary change from the

455   ancestral population occurred, and ii) experimental evolution under direct sexual selection

456   affected reproductive success differently than baseline selection alone (i.e., WS-P&P).

Genome sequencing, mapping, and SNP calling

458   We performed whole-genome sequencing on pooled samples of 2,000-3,000 L1 worms from

459   generations 0, 13, 22, and 31. Three independent pooled extractions were done for the ancestral

460   population (i.e., generation 0) to capture as many segregating variants as possible. Worms were

461   flash frozen and DNA was isolated using Genomic DNA Clean and Concentrator-10 (Zymo).

462   Libraries were prepared using the Nextera DNA Sample Prep kit (Illumina) starting from 5 ng of

463   DNA. 100 bp paired-end reads were sequenced on an Illumina HiSeq 4000 at the University of

464   Oregon Genomics and Cell Characterization Core Facility (Eugene, OR). The average genome-

465   wide sequencing coverage for generations 0, 13, 22, and 31 was 162×, 24×, 26×, 50×,

466   respectively.

467   Reads were trimmed using skewer v0.2.2 [51] to remove low quality bases (parameters: -

468   x CTGTCTCTTATA -t 12 -l 30 -r 0.01 -d 0.01 -q 20). The trimmed reads were mapped to the *C.*

469   *elegans* N2 reference genome (PRJNA13758-WS274) [30] using BWA-MEM v0.7.17

470   (parameters: -t 8 -M) [52] and then sorted using SAMtools v1.5 [53]. We removed PCR

471   duplicates with MarkDuplicates in Picard v2.6.0 (https://github.com/broadinstitute/picard),

472   realigned insertions/deletions with IndelRealigner in GATK v3.7

473   (https://github.com/broadinstitute/gatk/#authors), and called variants with mpileup in bcftools

474   v1.5 [54]. The mpileup file was then converted to a genotype-called vcf file, insertions/deletions

475   were removed, and the allelic depth was extracted for all biallelic SNPs for further analysis.

476   To improve the reliability of the analysis pipeline, additional filtering was done using R

477   [48]. Repeat regions were masked based the *C. elegans* N2 reference

478   (https://gist.github.com/danielecook/cfaa5c359d99bcad3200) and SNPs in the upper and lower

16

479 5% tails of the total coverage distribution (i.e., >342× and ≤20×, respectively) were removed.

480 This yielded a total of 326,648 SNPs to be considered for analyses.

Estimation and candidate SNP inference

482 Genetic diversity summary statistics were estimated for the ancestral population from 321,929

483 SNPs. Coverage-weighted average heterozygosity (π) was calculated following Begun et al. [55].

484 SNP density (θ_w) was calculated across 1kb sliding windows. We performed a Kolmogrov-

485 Smirnov test to determine if the site frequency spectrum, π, and θ_w differed between

486 chromosome arm domains and center domains [25]. Effective population size (N_e) was

487 calculated per chromosome for each of the evolved regime replicates following Waples [56] Plan

488 II sampling [57]. An analysis of variance was performed in R to determine if the genome-wide

489 N_e differed between regimes and Welch's Two-Sample t-test was performed to determine if the

490 estimated N_e on autosomes differed from the X chromosome. We estimated the upper bound on

491 the number of breeding males (N_m) by solving the equation $N_e = (4\ N_m\ N_f) / (N_m + N_f)$ for N_m

492 using the estimated effective population sizes and assuming that all females reproduced ($N_f =$

493 2,500).

494   Allele count data were analyzed using R [48] following two complementary models.

495 Model 1 fit allele counts for ancestral and evolved populations using a generalized linear mixed

496 model with a binomial logistic distribution: glm(SNP ~ regime). The SNP data going into Model

497 1 were filtered to ensure each SNP was present in the ancestor and at least ten of the evolved

498 replicates. A total of 263,373 SNPs fit the full model (File S4). The *multcomp* package [50] was

499 then used to perform a planned comparisons tests with defined contrasts to determine if

500 experimental evolution under direct sexual selection affects the genome differently than baseline

501 selection alone (i.e., WS-P&P). Model 2 fit allele counts across all time points for each regime

502 separately, again using a generalized linear mixed model with a binomial logistic distribution:

503 glm(SNP$_{regime}$ ~ time). The SNP data going into Model 2 were filtered to ensure each SNP was

504 present in the ancestor and at least nine occurrences across replicates and time points. A total of

505 202,926 SNPs, 222,731 SNPs, 200,324 SNPs, and 204,946 SNPs fit the full model for the WS-

506 P&P, WS-PO, BS-P&P, and BS-PO regimes, respectively (File S5). For both models,

507 significance was determined using a genome-wide Bonferroni cut-off.

508   A significance peak was called if five or more significant SNPs fell in a 1kb window.

509 Peaks were classified as occurring within a gene (intragenic) or between genes (intergenic) using

17

510 JBrowse in WormBase [30]. If multiple 1kb windows fell within a single gene, then the windows

511 were combined and called as a single intragenic peak. The molecular and biological functions of

512 the associated genes were determined using gene ontology analysis in UniProt [58] and

513 QuickGO [59].

Data accessibility

515 The oligonucleotides and synthetic constructs used in this study are available in Tables S1-S3.

516 The fertility data are available in File S7. The sequence data will be made publicly available on

517 NCBI prior to publication. Model summary statistics for the genomic analyses are available in

518 Files S1-S6. All R scripts are available via the GitHub public repository

519 https://github.com/katjakasimatis/postinsemination_expevol. Worm strains PX624, PX631, and

520 PX658 will be made available from the *Caenorhabditis* Genetics Center. All other strains are

521 available from the Phillips Lab upon request.

522

523

524

Acknowledgements

531

532

Funding

536

537

18

Author contributions

KRK and PCP devised the project. KRK and MJMS created the strains. KRK collected the experimental evolution data with assistance from RL and AS. JHW prepared the genomic libraries. KRK analyzed the data. KRK and PCP wrote the manuscript with the support of the other authors.

References

1.   Andersson M. Sexual Selection. New York: Princeton University Press; 1994.

2.   Lewontin R. The units of selection. Annu Rev Ecol Syst. 1970;1: 1–18.

3.   Immler S, Otto SP. The Evolutionary Consequences of Selection at the Haploid Gametic Stage. Am Nat. 2018;192: 241–249.

4.   Lorch PD, Stephen Proulx, Rowe L, Day T. Condition-dependent sexual selection can accelerate adaptation. Evol Ecol Res. 2003;5: 867–881.

5.   Candolin U, Heuschele J. Is sexual selection beneficial during adaptation to environmental change? Trends Ecol Evol. 2008;23: 446–452.

6.   Lande R. Models of speciation by sexual selection on polygenic traits. Proc Natl Acad Sci USA. 1981;78: 3721–3725.

7.   Arnold SJ, Wade MJ. On the measurement of natural and sexual selection: theory. Evolution. 1984;38: 709–719.

8.   Evans JP, Garcia-Gonzalez F. The total opportunity for sexual selection and the integration of pre- and post-mating episodes of sexual selection in a complex world. J Evol Biol. 2016;29: 2338–2361.

9.   Pischedda A, Rice WR. Partitioning sexual selection into its mating success and fertilization success components. Proc Natl Acad Sci USA. 2012;109: 2049–2053.

10.   Rose E, Paczolt KA, Jones AG. The contributions of premating and postmating selection episodes to total selection in sex-role-reversed Gulf pipefish. Am Nat. 2013;182: 410–420.

11.   Marie-Orleach L, Janicke T, Vizoso DB, David P, Schärer L. Quantifying episodes of sexual selection: Insights from a transparent worm with fluorescent sperm. Evolution. 2016;70: 314–328.

568 12. Devigili A, Evans JP, Di Nisio A, Pilastro A. Multivariate selection drives concordant
569   patterns of pre- and postcopulatory sexual selection in a livebearing fish. Nat Commun.
570   2015;6: 1–9.

571 13. Collet J, Richardson DS, Worley K, Pizzari T. Sexual selection and the differential effect
572   of polyandry. Proc Natl Acad Sci USA. 2012;109: 8641–8645.

573 14. Turnell BR, Shaw KL. High opportunity for postcopulatory sexual selection under field
574   conditions. Evolution. 2015;69: 2094–2104.

575 15. Pélissié B, Jarne P, Sarda V, David P. Disentangling precopulatory and postcopulatory
576   sexual selection in polyandrous species. Evolution. 2014;68: 1320–1331.

577 16. Begun DJ, Whitley P, Todd BL, Waldrip-Dail HM, Clark AG. Molecular population
578   genetics of male accessory gland proteins in *Drosophila*. Genetics. 2000;156: 1879–1888.

579 17. Swanson WJ, Vacquier VD. Reproductive Protein Evolution. Annu Rev Ecol Syst.
580   2002;33: 161–179.

581 18. Stewart AD, Phillips PC. Selection and maintenance of androdioecy in *Caenorhabditis
582   elegans*. Genetics. 2002;160: 975–982.

583 19. Kasimatis KR, Moerdyk-Schauwecker MJ, Phillips PC. Auxin-mediated sterility
584   induction system for longevity and mating studies in *Caenorhabditis elegans*. G3. 2018;8:
585   2655–2662.

586 20. Schlötterer C, Kofler R, Versace E, Tobler R, Franssen SU. Combining experimental
587   evolution with next-generation sequencing: a powerful tool to study adaptation from
588   standing genetic variation. Heredity. 2015;114: 431–440.

589 21. Teotonio H, Estes S, Phillips PC, Baer CF. Experimental Evolution with *Caenorhabditis*
590   Nematodes. Genetics. 2017;206: 691–716.

591 22. Seidel HS, Ailion M, Li J, van Oudenaarden A, Rockman MV, Kruglyak L. A novel
592   sperm-delivered toxin causes late-stage embryo lethality and transmission ratio distortion
593   in *C. elegans*. PLoS Biol. 2011;9: e1001115–21.

594 23. Gengyo-Ando K, Mitani S. Characterization of mutations induced by ethyl
595   methanesulfonate, UV, and trimethylpsoralen in the nematode *Caenorhabditis elegans*.
596   Biochem Biophy Res Commun. 2000;269: 64–69.

597 24. Cutter AD, Baird SE, Charlesworth D. High nucleotide polymorphism and rapid decay of
598   linkage disequilibrium in wild populations of *Caenorhabditis remanei*. Genetics.
599   2006;174: 901–913.

600 25. Rockman MV, Kruglyak L. Recombinational Landscape and Population Genomics of
601   *Caenorhabditis elegans*. PLoS Genetics. 2009;5: e1000419–16.

602   26.   Lee D, Zdraljevic S, Stevens L, Wang Y, Tanny RE, Crombie TA, et al. Balancing
603   selection maintains ancient genetic diversity in *C. elegans*. bioRxiv. 2020: 1–41.
604   doi:10.1101/2020.07.23.218420

605   27.   Andersen EC, Gerke JP, Shapiro JA, Crissman JR, Ghosh R, Bloom JS, et al.
606   Chromosome-scale selective sweeps shape *Caenorhabditis elegans* genomic diversity. Nat
607   Rev Genet. 2012;44: 285–290.

608   28.   Lande R. Sexual dimorphism, sexual selection, and adaptation in polygenic characters.
609   Evol. 1980;34: 292–305.

610   29.   Crow JF, Kimura M. An introduction to population genetics theory. New York: Harper
611   and Rowe; 1970.

612   30.   Harris TW, Arnaboldi V, Cain S, Chan J, Chen WJ, Cho J, et al. WormBase: a modern
613   Model Organism Information Resource. Nucleic Acids Res. 2019;gkz920.

614   31.   Holland B, Rice WR. Experimental removal of sexual selection reverses intersexual
615   antagonistic coevolution and removes a reproductive load. Proc Natl Acad Sci USA.
616   1999;96: 5083–5088.

617   32.   Mackay TFC, Stone EA, Ayroles JF. The genetics of quantitative traits: challenges and
618   prospects. Nat Rev Genet. 2009;10: 565–577.

619   33.   Otte KA, Nolte V, Mallard F, Schlötterer C. The adaptive architecture is shaped by
620   population ancestry and not by selection regime. bioRxiv. 2020;1–38.
621   doi:10.1101/2020.06.25.170878

622   34.   Kipreos ET, Pagano M. The F-box protein family. Genome Biol. 2000;1: 3002.1–3002.7.

623   35.   Ma F, Lau CY, Zheng C. Large genetic diversity and strong positive selection in F-box
624   and GPCR genes among the wild isolates of *Caenorhabditis elegans*. Genome Biol Evol.
625   2021;13: evab048.

626   36.   Charlesworth B. Fundamental concepts in genetics: effective population size and patterns
627   of molecular evolution and variation. Nat Rev Genet. 2009;10: 195–205.

628   37.   Corl A, Ellegren H. The genomic signature of sexual selection in the genetic diversity of
629   the sex chromosomes and autosomes. Evol. 2012;66: 2138–2149.

630   38.   Dickinson DJ, Pani AM, Heppert JK, Higgins CD, 2015. Streamlined genome engineering
631   with a self-excising drug selection cassette. Genetics. 2015;200: 1035–1049.

632   39.   Doench JG, Fusi N, Sullender M, Hegde M, Vaimberg EW, Donovan KF, et al. Optimized
633   sgRNA design to maximize activity and minimize off-target effects of CRISPR-Cas9. Nat
634   Biotechnol 2016 34:3. 2016;34: 184–191.

635 40. Hsu PD, Scott DA, Weinstein JA, Ran FA, Konermann S, Agarwala V, et al. DNA
636   targeting specificity of RNA-guided Cas9 nucleases. Nat Biotechnol 2016 34:3. 2013;31:
637   827–832.

638 41. Xu H, Xiao T, Chen C-H, Li W, Meyer CA, Wu Q, et al. Sequence determinants of
639   improved CRISPR sgRNA design. Genome Res. 2015;25: 1147–1157.

640 42. Dickinson DJ, Ward JD, Reiner DJ, Goldstein B. Engineering the *Caenorhabditis elegans*
641   genome using Cas9-triggered homologous recombination. Nat Meth. 2013;10: 1028–
642   1034.

643 43. Frøkjær-Jensen C, Davis MW, Ailion M, Jorgensen EM. Improved Mos1-mediated
644   transgenesis in *C. elegans*. Nat Meth. 2012;9: 117–118.

645 44. Paix A, Folkmann A, Rasoloson D, Seydoux G. High efficiency, homology-directed
646   genome editing in *Caenorhabditis elegans* using CRISPR-Cas9 ribonucleoprotein
647   complexes. Genetics. 2015;201: 47–54.

648 45. Stevenson ZC, Moerdyk-Schauwecker MJ, Jamison B, Phillips PC. Rapid self-selecting
649   and clone-free integration of transgenes into engineered crispr safe harbor locations in
650   *Caenorhabditis elegans*. G3. 2020;10: 3775–3782.

651 46. Brenner S. The genetics of *Caenorhabditis elegans*. Genetics. 1974;77: 71–94.

652 47. Kenyon C. The nematode *Caenorhabditis elegans*. Science. 1988;240: 1448–1453.

653 48. R Core Team. R: A language and environment for statistical computing [Internet]. Vienna,
654   Austria: Foundation for Statistical Computing; 2020. Available: https://www.R-
655   project.org/

656 49. Bates D, Mächler M, Bolker B, Walker S. Fitting linear mixed-effects models using lme4.
657   J Stat Soft. 2015;67: 1–48.

658 50. Hothorn T, Bretz F, Westfall P. Simultaneous inference in general parametric models.
659   Biom J. 2008;50: 346–363.

660 51. Jiang H, Lei R, Ding S-W, Zhu S. Skewer: a fast and accurate adapter trimmer for next-
661   generation sequencing paired-end reads. BMC Bioinformatics. 2014;15: 182–12.

662 52. Li H. Aligning sequence reads, clone sequences and assembly contigs with BWA-MEM.
663   arXiv. 2013;1303.3997v2: 1–3.

664 53. Li H, Handsaker B, Wysoker A, Fennell T, Ruan J, Homer N, et al. The Sequence
665   Alignment/Map format and SAMtools. Bioinformatics. 2009;25: 2078–2079.

666 54. Danecek P, Schiffels S, Durbin R. Multiallelic calling model in bcftools (-m). 2016.
667   Available at: http://samtools.github.io/bcftools/call-m.pdf

668   55.   Begun DJ, Holloway AK, Stevens K, Hillier LW, Poh Y-P, Hahn MW, et al. Population
669   genomics: whole-genome analysis of polymorphism and divergence in *Drosophila*
670   *simulans*. PLoS Biol. 2007;5: e310.

671   56.   Waples RS. A generalized approach for estimating effective population size from
672   temporal changes in allele frequency. Genetics. 1989;121: 379–391.

673   57.   Jónás Á, Taus T, Kosiol C, Schlötterer C, Futschik A. Estimating the effective population
674   size from temporal allele frequency changes in experimental evolution. Genetics.
675   2016;204: 723–735.

676   58.   UniProt Consortium. UniProt: the universal protein knowledgebase in 2021. Nucleic
677   Acids Res. 2021;49: D480–D489.

678   59.   Huntley RP, Sawford T, Mutowo-Meullenet P, Shypitsyna A, Bonilla C, Martin MJ, et al.
679   The GOA database: gene ontology annotation updates for 2015. Nucleic Acids Res.
680   2015;43: D1057–63.

681

Figures
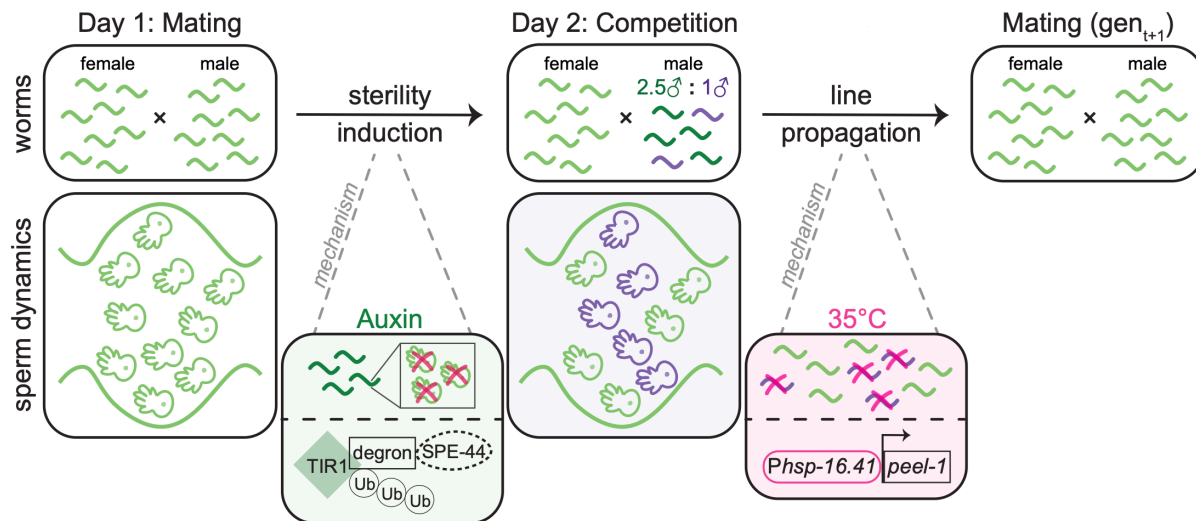
Fig 1. Day-by-day depiction of the experimental evolution design shown at the population level and at the sperm level. On day 1 sterility is induced by transferring worms to auxin-containing media. Auxin activates TIR1 to target the degron tag on SPE-44. The depletion of SPE-44 stops the production of sperm thereby inducing sterility. On day 2, competitor males are added to the population at a ratio of 1 competitor male to 2.5 evolving males. Progeny are collected on day 3 and heat-shocked on day 4 to induce ectopic expression of the toxic protein PEEL-1. This expression kills competitor cross-progeny, leaving only the progeny from sperm transferred during the day 1 mating phase. Each selective event is followed by a recovery generation.

24

694

25
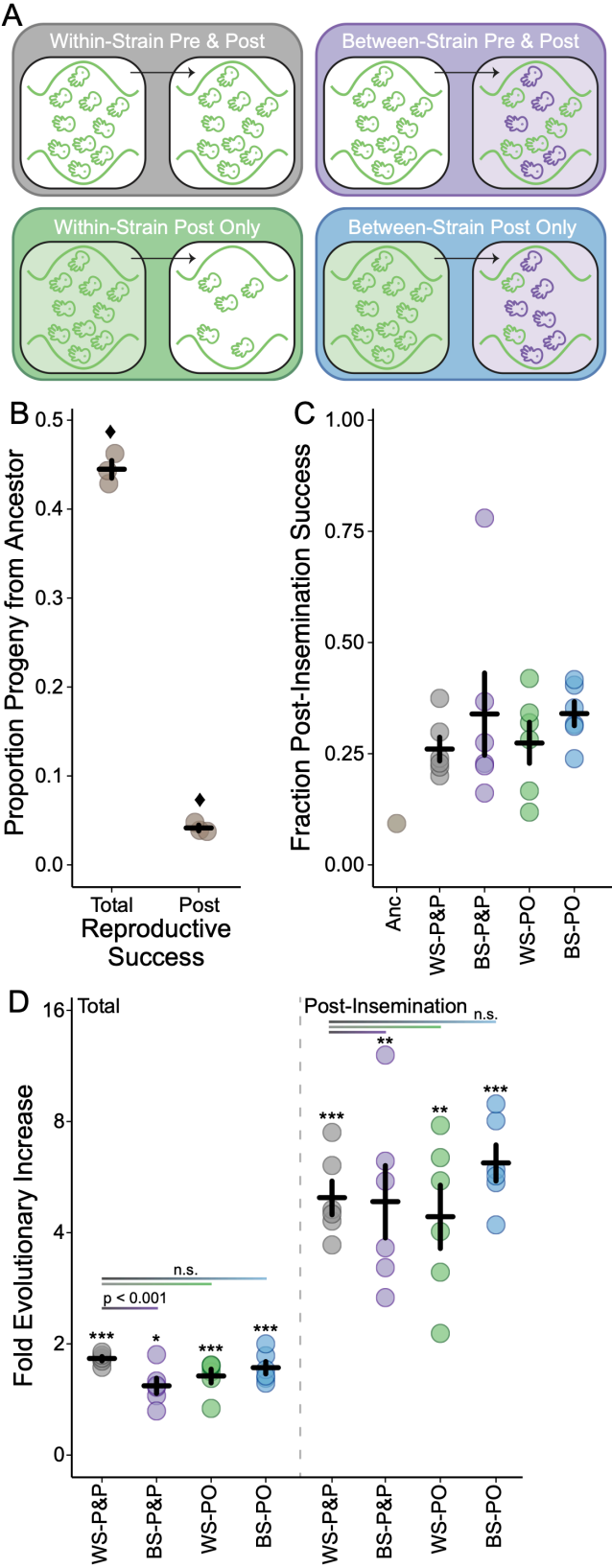
695 **Fig 2. The competitive reproductive success of males before and after experimental**

696 **evolution under four sexual selection regimes. A)** Partitioning the sterility and competition

697 treatments leads to four experimental evolution regimes: within-strain pre- and post-insemination

698 competition (WS-P&P, gray), within-strain post-insemination only competition (WS-PO, green),

699 between-strain pre- and post-insemination competition (BS-P&P, purple), and between-strain

700 post-insemination only competition (BS-PO, blue). **B)** Ancestral males have poorer reproductive

701 success than competitor males under both pre- and post-insemination competitive conditions

702 (total) and under only post-insemination competitive conditions. Each point represents an

703 independent assay with the mean and standard error across assays given. Diamonds denote a

704 significant deviation from the null hypothesis of equal competitive ability between ancestral and

705 competitive males for each condition (total: $\chi^2 = 6.87$, d.f. = 1, $p < 0.01$, 95% C.I. of ancestral

706 competitive success = 40.4–48.6%; post-insemination: $\chi^2 = 863$, d.f. = 1, $p < 0.0001$, 95% C.I. of

707 ancestral sperm competitive success = 3.0–5.5%). **C)** The fraction of total reproductive success

708 attributable to post-insemination success in the ancestral population (Anc) and the evolved

709 populations (WS-P&P, BS-P&P, WS-PO, BS-PO). Each point represents a mean of three

710 independent assays for the ancestor and each evolved replicate with the mean and standard error

711 across evolved replicates shown. **D)** The fold change in the total reproductive success and the

712 post-insemination reproductive success of males in the evolved regimes relative to the ancestor

713 (plotted on a $\log_2$ scale). Males in all regimes significantly increased in both measures of

714 reproductive success (*$p < 0.05$, **$p < 0.01$, ***$p < 0.001$). Post hoc tests for a difference

715 between the WS-P&P and the BS-P&P, WS-PO, and BS-PO regimes are indicated by the

716 horizontal lines. The only significant difference appears between the total reproductive success

717 of the WS-P&P and BS-P&P regimes, in which pre-insemination competition reduces the

718 evolutionary response. Each point represents a mean of three independent assays for each

719 evolved replicate with the mean and standard error across replicates shown.

720

26
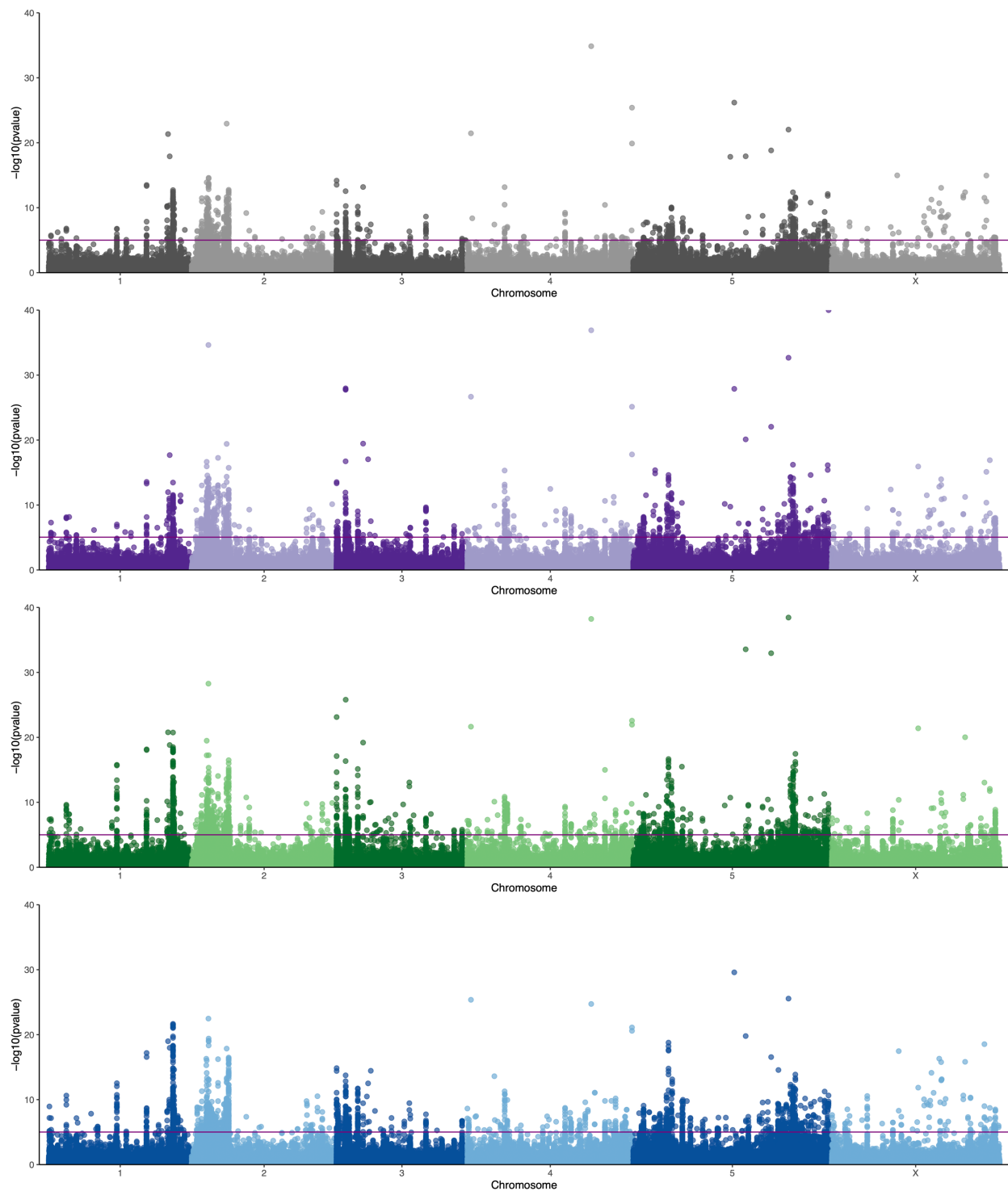
Fig 3. Genomic response for each SNP over time fit for each regime (Model 2). The horizontal line represents the Bonferroni significance threshold. Reproductive success is a highly polygenic trait with 49 peaks identified in the WS-P&P regime (gray), 77 in the BS-P&P regime

725   (purple), 102 in the WS-PO regime (green), and 107 in the BS-PO regime (blue). The

726   distribution of peak overlaps in shown in Figure S3.

Supporting information

S1 Fig. Schematic of strain construction. A) The components for creating an obligate outcrossing sterility induction line were genetically engineered in the wild isolate background JU2526. The spermatogenesis gene *spe-44* was degron-tagged and TIR1 was inserted to create strain PX737. The hermaphrodite self-sperm gene (*fog-2*) was knocked-out to create strain PX738. These strains are used in panels C and D. **B)** To generate an inducible lethality line, heat-shock driven *peel-1* was inserted into the CB4856 background on Chromosomes I and II to create strains PX739 and PX630, respectively. These strains are used in panels D and E. **C)** Strains PX737 and PX738 were crossed to creating a male-female, inducible sterility triple mutant (PX624). Strain PX624 went through five low dose rounds of mutagenesis each followed by two recovery generations. After the final recovery generation, the population was expanded for 15 generations of lab adaptation to create the experimental evolution ancestral population (PX632). **D)** The competition strain has five transgenic modifications. Heat-shock driven *peel-1* was inserted on Chromosome III of strain PX737, creating an inducible lethality and inducible sterility strain (PX656). Strains PX624 and PX631 (panel E) were crossed to given another inducible lethality and sterility double mutant. These worms were backcrossed to PX624 five times to give a predominantly JU2526 genomic background. This strain, PX655, was crossed with PX656 yielding a quintuple mutant, which was inbred to three generations followed by five generations of lab adaptation. The final strain PX658 served as the competitor during experimental evolution. **E)** A separate bioassay competitor strain was generated by introgressing the *fog-2*(q71) mutation into PX739. These worms were backcrossed to the CB4856 genomic background four times and then inbred for 14 generations, creating strain PX626. This strain was crossed to PX630 to create an obligate outcrossing strain with two heat-shock driven *peel-1* insertions. The final strain PX631 served as the novel competitor during phenotypic assays.

S2 Fig. Genetic diversity of the ancestral population. A) The minor allele frequency (MAF) across Chromosome II (as an exemplar). The genome-wide mean is shown in blue. **B)** Histogram of MAF counts across the entire genome binned by chromosome arms and chromosome center. Values of zero are excluded from the plot. **C)** Nucleotide diversity (π) calculated per SNP across Chromosome II. The genome-wide mean is shown in blue. **D)** Histogram of nucleotide diversity across the entire genome binned by chromosome arms and chromosome center. Values of zero

29

758   are excluded from the plot. **E)** SNP density (θ_w) per base pair across Chromosome II. The

759   genome-wide mean is shown in blue. **F)** Histogram of SNP density in 1kb windows across the

760   entire genome binned by chromosome arms and chromosome center.

761

762   **S3 Fig. The estimated effective population size (N_e) per chromosome for all replicates.** The

763   effective population size was greatly reduced compared to the census size (N = 5,000). Regime

764   did not have a significant effect on effective population size (F = 0.72, d.f. = 3, p = 0.54).

765

766   **S4 Fig. Breakdown of significance peaks from Model 2.** The counts of significance peaks are

767   shown along with the combination of regimes contributing to that count. Unique peaks are

768   represented by a single black dot for the given regime. Shared peaks have multiple connected

769   black dots. The total number of significant SNPs within each regime is given.

770

771   **S5 Fig. Zoom plot of the major significance peak on the right arm of Chromosome I.**

772   Significant SNPs pile up in the second intron of gene C17H1.2. This gene has male-biased

773   expression, though it's function is uncharacterized.

774

775   **S6 Fig. The molecular functions for genes associated with significance peaks based on a GO**

776   **analysis.** Ubiquitin ligase complex formation through F-box proteins, carbohydrate binding, G-

777   coupled protein receptor activity, and transferase transporter activity were the most common

778   functions identified. However, the majority of genes are yet uncharacterized in function.

779

780   **S1 Table. Guide sequences.** The guide sequence, genomic location, target region/gene, and

781   format (plasmid or cr:tracrRNA) are given.

782

783   **S2 Table. Plasmid construction.** The plasmid name and insert are given for both plasmids used

784   in construction and as repair templates.

785

786   **Table S3. Primers.** The primer name, sequence (in 5' to 3' orientation), and purpose for a given

787   primer are listed.

788

789 **Table S4. Strains generated in this study.** Full genotype information for each strain used in

790 this study, along with the genomic background, method of construction, and generations of

791 backcrossing and/or inbreeding.

792

793 **S1 File. SNP data for the ancestor.** The chromosome, position (in base pairs), reference allele,

794 alternate allele, counts of reference alleles, counts of alternate alleles, total coverage, minor allele

795 frequency (MAF), chromosome domain, and nucleotide diversity (π) are given.

796

797 **S2 File. Watterson's theta calculated in 1kb windows across each chromosome.** The

798 chromosome, chromosome domain, theta per window, and theta per base pair are given.

799

800 **S3 File. Effective population size estimated using Waples Plan II sampling for each**

801 **replicate and each chromosome.**

802

803 **S4 File. Summary statistics for the Model 1 planned comparison analysis of ancestral**

804 **versus evolved allele counts.** For each SNP, the chromosome and position (in base pairs) is

805 given along with the slope estimate and p-value for each regime comparison.

806

807 **S5 File. Summary statistics for the Model 2 GLM analysis of allele counts over time for**

808 **each regime.** For each SNP within each regime, the chromosome and position (in base pairs) is

809 given along with the model intercept, slope estimate, standard error, z-value, and p-value.

810

811 **S6 File. Summary of the significance peaks identified using the Model 2 genomic results.**

812 The chromosome, start position (in base pairs), stop position (in base pairs), presence in each

813 treatment, associated gene, genetic region, molecular function (from GO analysis), and

814 biological function (from GO analysis) are given.

815

816 **S7 File. Competitive phenotyping data for the ancestor and all evolved replicates.**